

Retrieval of Ice Cloud Optical Thickness and Effective Particle Size Using a Fast Infrared Radiative Transfer Model

CHENXI WANG,* PING YANG,* BRYAN A. BAUM,⁺ STEVEN PLATNICK,[#] ANDREW K. HEIDINGER,[@]
YONGXIANG HU,[&] AND ROBERT E. HOLZ⁺

* *Department of Atmospheric Sciences, Texas A&M University, College Station, Texas*

⁺ *Space Science and Engineering Center, University of Wisconsin—Madison, Madison, Wisconsin*

[#] *NASA Goddard Space Flight Center, Greenbelt, Maryland*

[@] *NOAA/NESDIS Center for Satellite Applications and Research, Madison, Wisconsin*

[&] *NASA Langley Research Center, Hampton, Virginia*

(Manuscript received 23 March 2011, in final form 23 June 2011)

ABSTRACT

A computationally efficient radiative transfer model (RTM) is developed for the inference of ice cloud optical thickness and effective particle size from satellite-based infrared (IR) measurements and is aimed at potential use in operational cloud-property retrievals from multispectral satellite imagery. The RTM employs precomputed lookup tables to simulate the top-of-the-atmosphere (TOA) radiances (or brightness temperatures) at 8.5-, 11-, and 12- μm bands. For the clear-sky atmosphere, the optical thickness of each atmospheric layer resulting from gaseous absorption is derived from the correlated- k -distribution method. The cloud reflectance, transmittance, emissivity, and effective temperature are precomputed using the Discrete Ordinate Radiative Transfer model (DISORT). For an atmosphere containing a semitransparent ice cloud layer with a visible optical thickness τ smaller than 5, the TOA brightness temperature differences (BTDs) between the fast model and the more rigorous DISORT results are less than 0.1 K, whereas the BTDs are less than 0.01 K if τ is larger than 10. With the proposed RTM, the cloud optical and microphysical properties are retrieved from collocated observations from the Moderate Resolution Imaging Spectroradiometer (MODIS) and Cloud-Aerosol Lidar with Orthogonal Polarization (CALIOP) in conjunction with the Modern Era Retrospective-Analysis for Research and Applications (MERRA) data. Comparisons between the retrieved ice cloud properties (optical thickness and effective particle size) based on the present IR fast model and those from the *Aqua*/MODIS operational collection-5 cloud products indicate that the IR retrievals are smaller. A comparison between the IR-retrieved ice water path (IWP) and CALIOP-retrieved IWP shows robust agreement over most of the IWP range.

1. Introduction

Numerous approaches (e.g., Nakajima and King 1990; Stubenrauch et al. 1999; Platnick et al. 2003; Chiriaco et al. 2004; Kokhanovsky and Nauss 2005; Minnis et al. 2011a,b) have been developed to infer ice cloud optical thickness τ , effective particle size D_{eff} , and the ice particle size distribution function (PSD; e.g., Mitchell et al. 2010) from satellite-based imager and hyperspectral infrared (IR) sounder measurements. The method used by the Moderate Resolution Imaging Spectroradiometer

(MODIS) operational cloud-property retrieval is a bispectral method employing solar-reflectance bands (Platnick et al. 2003). The premise of this approach is that a weakly absorbing, visible or near-infrared window band (VIS/NIR) (e.g., 0.64 or 0.86 μm) is sensitive mainly to τ , whereas an ice absorbing shortwave infrared (SWIR) band (e.g., 1.6 or 2.13 μm) is sensitive to both D_{eff} and τ . To be more specific, in a VIS band, scattering is dominant so that the reflectance is primarily dependent on τ . For a SWIR channel, for which both scattering and absorption are important, the single-scattering albedo decreases and the asymmetry factor increases with an increase of D_{eff} , which results in reflectance being highly sensitive to D_{eff} in the SWIR region. The ice cloud properties can be inferred from radiance measurements based on lookup tables (LUT) that include the transmittance

Corresponding author address: Prof. Ping Yang, Dept. of Atmospheric Sciences, Texas A&M University, College Station, TX 77843.

E-mail: pyang@tamu.edu

and reflectance functions for clouds of various viewing geometries, surface boundary conditions, τ , and D_{eff} . Figure 1 shows an example of an LUT for a pair of MODIS bands at 0.86 and 2.13 μm . This approach works best when the isolines of τ and D_{eff} in the $R_{0.86}$ – $R_{2.13}$ (here the terms indicate the reflectances at 0.86- and 2.13- μm bands) space are orthogonal, which tends to occur when $\tau > 4$. At lower values of τ , the isolines begin to converge, coupling the τ and D_{eff} solution. Furthermore, as τ decreases below 4, the retrievals become increasingly sensitive to surface albedo characteristics, that is, the clear-sky values for the VIS/NIR and SWIR bands. Because VIS/NIR and SWIR channels are involved, this method is limited to daytime retrievals in which the solar zenith angle θ_o is less than $\sim 82^\circ$ [i.e., $\cos(\theta_o) \geq 0.15$]. In addition, as shown in several previous studies (e.g., Hess et al. 1998; Sun et al. 2004; Yang et al. 2008; Baum et al. 2010), the single-scattering properties in the solar bands are sensitive to the assumed ice habit and the degree of ice particle surface roughening, and these effects influence the LUT.

Another approach to inferring τ and D_{eff} is the split-window technique (Inoue 1985), which is based on two IR-window channels (i.e., 11 and 12 μm). The premise for this method is that the absorption characteristics of ice are different at wavelengths 11 and 12 μm (Prabhakara et al. 1988). This is the approach adopted for the decadal “climatology” that is based on the Advanced Very High Resolution Radiometer (Heidinger and Pavolonis 2009). The split-window method is sensitive to optically thin ice clouds for which $0.5 < \tau < 5$ and, as such, is complementary to the solar-reflectance method adopted by MODIS. Another benefit is that an IR-based approach can be applied to all data regardless of solar illumination, leading to consistent retrievals for both daytime and nighttime conditions, a distinct advantage for building an ice cloud climatology. Furthermore, the ice crystal optical properties (Baran 2004, 2009; Yang et al. 2005, and references cited therein) used to generate the LUTs are fundamental to ice cloud-property retrievals (Chepfer et al. 1998; Wendisch et al. 2005; Yang et al. 2007), and it is very challenging to simulate realistic ice crystal shapes and surface textures (i.e., the degree of surface roughness) in light-scattering calculations. The LUTs based on IR bands are insensitive to ice particle surface roughness.

An accurate and computationally efficient radiative transfer (RT) model for cloudy conditions is indispensable for an IR retrieval algorithm. Among the available rigorous RT models that consider multiple scattering are the Discrete Ordinate Radiative Transfer model (DISORT; Stamnes et al. 1988), the Monte Carlo method (Collins et al. 1972; Plass and Kattawar 1968), and the

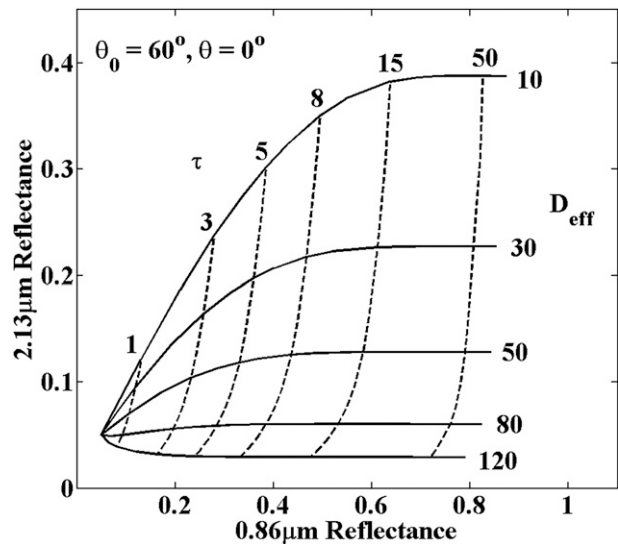


FIG. 1. Relationship between 0.86- and 2.13- μm reflectance functions for ice clouds. Surface albedo is 0.05 (for two bands), solar zenith angle is 60° , and view zenith angle is 0° . Solid lines are lines of constant D_{eff} , and dashed lines are lines of constant τ .

adding–doubling method (Twomey et al. 1966; Hansen and Hovenier 1971). These methods are developed for scientific research rather than operational applications, however. For this reason, a computationally efficient RT model is desirable for generating operational satellite data products.

In recent years, development has progressed on new fast models that rely on parameterizations to speed up the computations. For example, the Radiative Transfer for the Television Infrared Observation Satellite (TIROS) Operational Vertical Sounder (TOVS) (RTTOV; Saunders et al. 1999, 2006) is a fast RT model developed for space-based multisensors and can be coupled with a numerical weather prediction model. The Principal Component–Based Radiative Transfer Model (PCRTM; Liu et al. 2006), the optical path transmittance (OPTRAN; McMillin et al. 1995) algorithm, correlated- k distribution (CKD; Kratz 1995; Kratz and Rose 1999), and the optimal spectral sampling (Moncet et al. 2008) method are designed to minimize the computational effort for high-spectral-radiance simulation, especially for molecular-absorption simulations. Dubuisson et al. (2005) developed a fast RT model to simulate top-of-the-atmosphere (TOA) brightness temperatures (BTs) for clear or water-cloudy atmospheres. Heidinger et al. (2006) developed the Successive Order of Interaction model by implementing several approximations to the adding–doubling method that are most applicable to moderately scattering atmospheres in the IR and microwave regions. Zhang et al. (2007) developed a flexible adding–doubling-based

fast RT model (FIRTM-AD) that could be applied to an atmosphere with an arbitrary number of cloud and aerosol layers with differing microphysical and optical properties. The FIRTM-AD could be used for analysis of both space-based and ground-based high-spectral-resolution radiance observations. The root-mean-square (RMS) brightness temperature differences (BTDs) were smaller than 0.1 K in comparisons with rigorous DISORT results, but the FIRTM-AD performed similar calculations 250 times as fast as DISORT. For hyperspectral IR calculations, Wei et al. (2004) reported the development of the FIRTM1, and Niu et al. (2007) developed the next generation of the model (FIRTM2). The RT calculations involving FIRTM2 are faster than DISORT by three orders of magnitude. Because these models assume clouds to be homogenous and isothermal, however, the accuracy of the simulated results decreases slightly. The RMS of the TOA BTDs between the FIRTM1/FIRTM2 and DISORT can be as high as 0.5 K, which means these two models are not accurate enough for cloud retrievals. Hong et al. (2007) reported that consideration of the cloud geometrical thickness—essentially the nonisothermal effect of clouds—improves the radiative transfer model (RTM) simulation.

This paper explores the development of a computationally efficient RTM for the inference of τ and D_{eff} from satellite-based IR radiance measurements, specifically at three spectral bands centered at 8.5, 11, and 12 μm . For an atmosphere containing a semitransparent ice cloud layer with a visible (0.65 μm) τ that is smaller than 5, the BTDs between the fast model and the more rigorous DISORT results are less than 0.1 K, whereas the BTDs are less than 0.01 K when the τ value exceeds 5. When compared with FIRTM-AD, the present model simulations for single-layered ice clouds show similar accuracy but with computational speed increased by an order of magnitude. Measurements at these specific wavelengths are currently available from satellite imagers such as MODIS and the Spinning Enhanced Visible and Infrared Imager (SEVIRI), as well as from hyperspectral IR sensors such as the Atmospheric Infrared Sounder (AIRS) and Infrared Atmospheric Sounding Interferometer. In the future, similar measurements will be provided by the Geostationary Operational Environmental Satellite (GOES-R) Advanced Baseline Imager, the Visible Infrared Imaging Radiometer Suite, and the Cross-track Infrared Scanner (CrIS).

This paper is organized into six sections. Section 2 introduces the basic method of the fast IR RTM. In section 3, the model simulation results are compared with DISORT. Section 4 is a sensitivity study conducted to assess the retrieval feasibility. In section 5, we present a retrieval method designed to simulate the ice cloud

properties and the retrieved results in comparison with MODIS collection-5 operational products. A discussion of the results and the conclusions of this study are given in section 6.

2. Method

The present fast RTM is developed to simulate TOA BTs of three IR wavelengths (8.5, 11, and 12 μm) for cloudy (ice phase) conditions. In the RTM implementation, the background atmosphere is assumed to be plane parallel but vertically inhomogeneous and can be divided into discrete homogeneous and isothermal clear atmosphere layers. A vertically homogeneous but nonisothermal ice cloud can be placed into an arbitrary layer in the atmosphere. For an ice cloud layer, the temperature within the cloud is assumed to decrease linearly with altitude. Thermal emission from the surface or a clear atmosphere layer is assumed to be isotropic. The molecular scattering under clear-sky conditions is neglected at these IR wavelengths. Furthermore, only the first-order reflected radiances between an ice cloud layer and the surface are considered; the emissivity and the ice cloud temperature are two independent parameters.

To consider the absorption of the background atmosphere, the CKD method is employed to derive the absorption optical thickness resulting from gaseous absorption. As for the ice cloud layer, both scattering and absorption processes are important. In this study, the ice cloud bulk scattering models are the narrowband models developed by Baum et al. (2005a,b). The averaged scattering properties are inferred from the single-scattering properties for six ice particle habits (Yang et al. 2000, 2005; Zhang et al. 2004) and from PSDs measured in situ (Heymsfield et al. 2002).

As shown in Fig. 2, the atmosphere is assumed to consist of $N - 1$ layers (i.e., $L_1, L_2, \dots, L_{M-1}, L_{M+1}, \dots, L_N$) with an ice cloud in layer L_M . Each clear atmospheric layer has a unique absorption optical thickness and a midlayer temperature, whereas an ice cloud layer is specified by four basic properties: cloud-top temperature T_{top} , cloud-base temperature T_{base} , τ , and D_{eff} . To consider nonisothermal ice cloud layers, we introduce a new physical quantity, effective temperature T_e , defined as

$$T_e = B^{-1}(I/\varepsilon), \quad (1)$$

where I is the emitted radiance from the cloud layer, ε indicates the cloud emissivity, and B^{-1} expresses the inversion of the Planck function. The ice cloud effective temperature, emissivity ε_c , reflectance r , and transmittance t functions are provided by four precomputed LUTs. Unless specifically stated, the ice cloud extinction

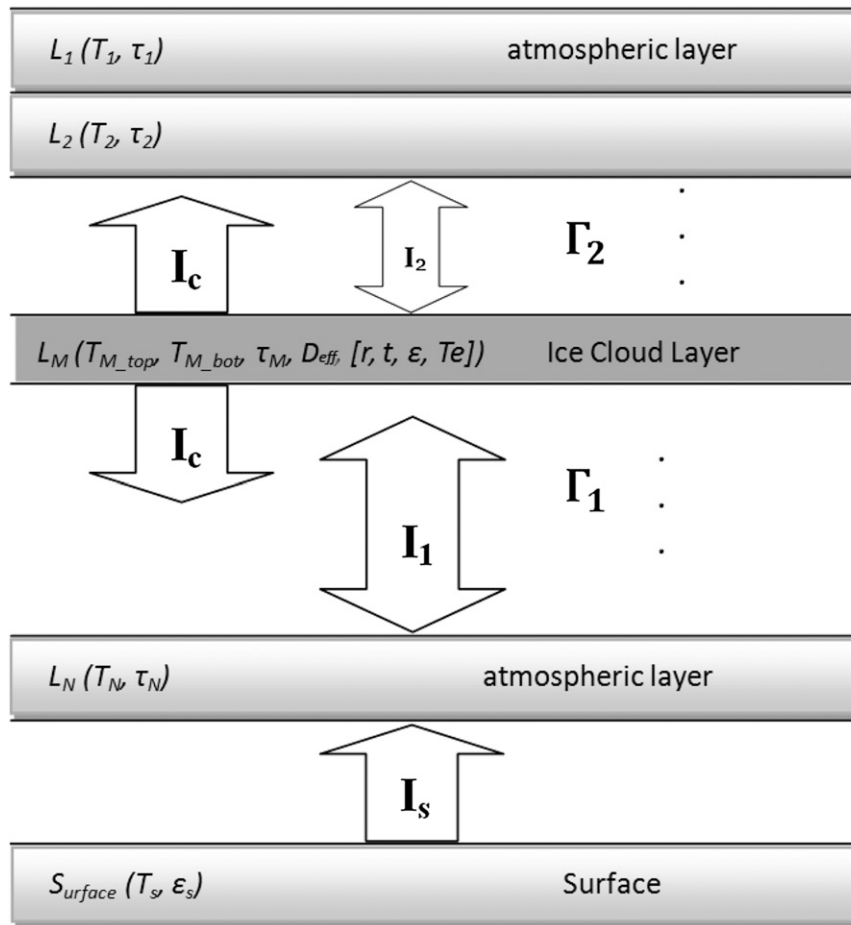


FIG. 2. Illustrative diagram of the fast IR RTM radiance components I for a single ice cloud in layer L_M , located between top and bottom layers L_1 and L_N , respectively.

optical thickness is referenced to a visible (VIS; $0.65 \mu\text{m}$) wavelength $\tau_{\text{ext,vis}}$. The ice cloud extinction optical thickness at an arbitrary wavelength λ ($\tau_{\text{ext},\lambda}$) can be derived as follows:

$$\tau_{\text{ext},\lambda} = \tau_{\text{ext,vis}} \frac{\langle Q_{\text{ext},\lambda} \rangle}{\langle Q_{\text{ext,vis}} \rangle}, \quad (2)$$

where $\langle Q_{\text{ext},\lambda} \rangle$ represents the bulk extinction efficiency at wavelength λ and $\langle Q_{\text{ext,vis}} \rangle$ is the bulk VIS extinction efficiency, both of which depend on the D_{eff} . It must be emphasized that, in this study, the effect of vertical inhomogeneity of D_{eff} is ignored. The definition of D_{eff} is expressed as follows (Mitchell 2002; Baum et al. 2003, and references cited therein):

$$D_{\text{eff}} = \frac{3 \int_{D_{\text{min}}}^{D_{\text{max}}} \left[\sum_{i=1}^N V_i(D) w_i(D) \right] n(D) dD}{2 \int_{D_{\text{min}}}^{D_{\text{max}}} \left[\sum_{i=1}^N A_i(D) w_i(D) \right] n(D) dD}, \quad (3)$$

where D is the maximum dimension of a single ice cloud particle, $V(D)$ is the volume of an ice crystal, $A(D)$ indicates the randomly oriented ice cloud particle projected area, subscript i denotes the particle habit index, and $n(D)$ and $w(D)$ are the size distribution and habit distribution.

In Eqs. (4) and (5), I_1 and I_2 indicate the thermal emission at the cloud layer from the lower and upper part of atmosphere, respectively, and I_c and I_s represent the emitted radiances from the ice cloud layer and the surface:

$$I_1 = \int_0^{\text{cloudbase}} B[T(z)] \frac{d\Gamma(z)}{dz} dz, \quad (4)$$

$$I_2 = \int_{\text{cloudtop}}^{\infty} B[T(z)] \frac{d\Gamma(z)}{dz} dz, \quad (5)$$

$$I_c = B(T_e) \epsilon_c, \quad \text{and} \quad (6)$$

$$I_s = B(T_s) \epsilon_s, \quad (7)$$

where $\Gamma(z)$ is the transmittance of atmosphere from TOA to altitude z , $B(T)$ is the Planck function at temperature T , and T_s and ε_s represent surface temperature and emissivity, respectively.

The TOA upward radiance I_{TOA} can be expressed as the sum of three parts: the direct transmission part of the thermal emission from the surface, ice cloud, and atmosphere I_A ; the first-order radiance reflected by the surface I_B ; and the first-order radiance reflected by the ice cloud (I_C):

$$I_A = I_s \Gamma_1 t \Gamma_2 + I_1^\uparrow t \Gamma_2 + I_c^\uparrow \Gamma_2 + I_2^\uparrow, \quad (8)$$

$$I_B = (I_1^\downarrow + I_c^\downarrow \Gamma_1 + I_2^\downarrow t \Gamma_1)(1 - \varepsilon_s) \Gamma_1 t \Gamma_2, \quad \text{and} \quad (9)$$

$$I_C = I_2^\downarrow r \Gamma_2, \quad (10)$$

where Γ_1 and Γ_2 are transmittances of lower and upper atmosphere and the arrow symbols “ \downarrow ” and “ \uparrow ” indicate the downwelling and upwelling radiances, respectively. The definition of the transmittances of the upper and lower parts of atmosphere is

$$\Gamma = \exp(-\tau_{\text{atm}}), \quad (11)$$

where τ_{atm} is the optical thickness of the background atmosphere.

To improve the computational efficiency and maintain the accuracy, the four LUTs (r , t , ε_c , and T_e functions) are generated with DISORT in the 32-stream mode. The band-averaged bulk scattering properties at 8.5, 11, and 12 μm (Baum et al. 2007) include the extinction efficiency factor, single-scattering albedo, and scattering phase function, all of which are used as input parameters in DISORT.

DISORT provides the r and t functions. The corresponding emissivity function can be expressed as follows, assuming an isothermal ice cloud layer with temperature T_c :

$$\varepsilon_c(\lambda, \tau, D_{\text{eff}}, \mu) = \frac{I_{\text{cloudtop}}(T_c, \lambda, \tau, D_{\text{eff}}, \mu)}{B(T_c, \lambda)}, \quad (12)$$

where μ indicates the cosine of the radiance zenith angle and I_{cloudtop} is the upwelling radiance at cloud top. Although both I_{cloudtop} and $B(T_c, \lambda)$ are temperature dependent, the emissivity function $\varepsilon_c(\lambda, \tau, D_{\text{eff}}, \mu)$ is relatively insensitive to temperatures between 200 and 260 K, the range that encompasses most atmospheric ice clouds. After generating the emissivity, T_e for a nonisothermal ice cloud (i.e., where the cloud temperature within a layer varies with height) can be expressed as follows:

$$T_e = \left\{ \frac{T_B \left[\frac{I(T', T'', \lambda, \tau, D_{\text{eff}}, \mu)}{\varepsilon_c(\lambda, \tau, D_{\text{eff}}, \mu)} \right] - T'}{T'' - T'} \right\} \times (T_{\text{base}} - T_{\text{top}}) + T_{\text{top}}, \quad (13)$$

where $T_B(I, \lambda)$ is the inverse Planck function, $I(T', T'', \lambda, \tau, D_{\text{eff}}, \mu)$ is the DISORT-computed thermal emission at the top (or bottom) of a nonisothermal ice cloud with an arbitrary cloud-top temperature T' and cloud-base temperature T'' and T_{base} and T_{top} are the actual temperature of the cloud base and cloud top.

For this study, a set of LUTs is derived for three MODIS infrared bands (i.e., 8.5, 11, and 12 μm), for 33 τ values ranging from 0.01 to 100, for 18 D_{eff} values ranging from 10 to 180 μm , and for nine satellite view zenith angles from 0° to 80° .

3. Comparisons between the fast RTM and DISORT

In this section, the accuracy of the fast RTM is evaluated by comparing the simulated TOA BTs with their DISORT counterparts. The comparisons are based on a generalized tropical atmosphere consisting of 100 parallel layers (101 levels) in which the geometrical thickness of the entire atmosphere is 100 km and the geometrical thickness of each layer varies from 0.5 km in the lower troposphere to 2.5 km at higher altitudes. Figure 3 shows the BTDs between these two models as a function of τ for the 8.5-, 11-, and 12- μm wavelengths. The BTD is defined as follows:

$$\text{BTD} = \text{BT}_{\text{fastmodel}} - \text{BT}_{\text{DISORT}}. \quad (14)$$

Each panel in Fig. 3 shows the comparisons of simulation results that are based on a surface emissivity of 1 and a viewing zenith angle of 20° . For an atmosphere containing a semitransparent ice cloud layer ($\tau < 5$), the BTDs are generally smaller than 0.1 K, except for small D_{eff} , and the error decreases rapidly to 0.01 K with increasing τ . We note that the simulation result has a higher accuracy in the 12- μm channel than in either the 8.5- or 11- μm channels. This may be due to the imaginary part of the ice refractive index increasing monotonically as a function of wavelength between 8.5 and 12 μm (Warren and Brandt 2008) and indicating that absorption is stronger at the longer wavelengths; that is, ice clouds are more opaque at longer wavelengths. As τ increases, the BTDs decrease to negligible values because opaque ice clouds behave almost like blackbodies. Furthermore, when a cloud is composed of primarily small ice particles (Figs. 3a,c) making the scattering

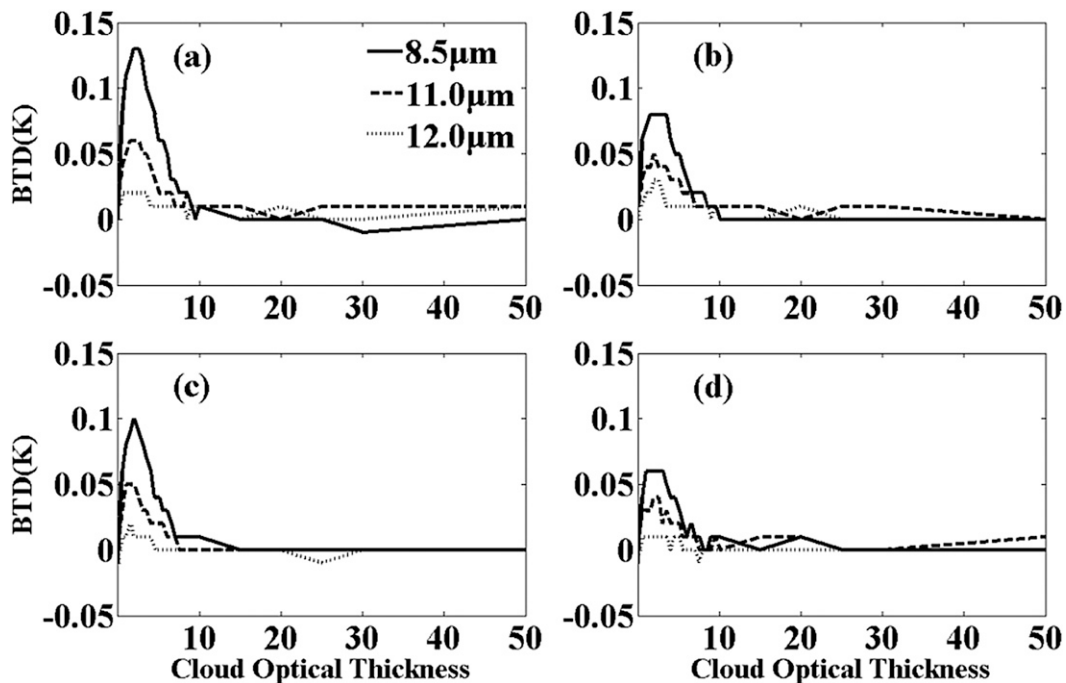


FIG. 3. Brightness temperature difference (DISORT – fast RTM) as a function of τ , for a view zenith angle of 20° for (a),(b) clouds located between 12 and 12.5 km and (c),(d) ice clouds located between 8 and 8.5 km for $D_{\text{eff}} =$ (left) 50 and (right) 80 μm .

processes relatively important, the simulation differences between the two models are relatively large, suggesting that the fast RTM does not capture scattering as accurately as DISORT does. In general, for an arbitrary viewing zenith angle, this model performs well (i.e., error < 0.1 K) when D_{eff} is larger than 30 μm and τ is larger than 5 (or smaller than 1). The largest error, 0.15 K, occurs when D_{eff} is smaller than 30 μm and τ is approximately 3. The reason for the relatively large error in this region needs further study. The fast RTM is much more computationally efficient than DISORT, however. For 16 038 cases (3 wavelengths, 33 optical thicknesses, 18 effective particle sizes, and 9 values of μ), more than 2 h on a Linux workstation (Dell, Inc., Power Edge R610) were required to simulate the TOA BTs using DISORT with 32 streams, whereas the fast RTM completed the same calculations in 1.5 s.

4. Sensitivity study

This section evaluates the feasibility of ice cloud inference of τ and D_{eff} using the fast RTM at 8.5-, 11-, and 12- μm wavelengths through a sensitivity study based on a tropical atmosphere containing ice clouds of different properties. The surface and cloud-top temperatures are 299.7 and 247 K, respectively. The μ is 1 (i.e., nadir

viewing conditions), and the surface emissivity is assumed to be 1. The simulated TOA BTs of an ice cloud with various D_{eff} values are shown in Fig. 4 as functions of τ . The seven color arches represent ice clouds with a set of D_{eff} values, ranging from 10 to 180 μm , and τ increases from 0 at the warmer temperatures to 100 at the colder temperatures. For each D_{eff} value, the TOA BT decreases rapidly with increasing τ until τ reaches a threshold value ($\tau \approx 7$) at which the cloud essentially becomes opaque. Moreover, for semitransparent cloud conditions, Fig. 4 shows that the TOA BTDs are highly sensitive to relatively small particle sizes ($D_{\text{eff}} < 80 \mu\text{m}$)—in particular, at the 8.5- μm wavelength.

If only TOA BTs (BTDs) are involved, however, the retrieved τ is more accurate than the retrieved D_{eff} under the same conditions. This may be due to the different sensitivities of a BT- τ pair and a BTD- D_{eff} pair, which can be inferred from comparing the ranges of TOA BTs and BTDs from Fig. 4. In general, BTs vary from approximately 250 to 300 K when τ decreases from 5 to 0, whereas the BTD ranges are limited to several kelvins even when the D_{eff} values change from 10 to 180 μm . This feature poses an obstacle to the retrieval of D_{eff} . For example, if the actual values of TOA BTs at 11 and 12 μm for an atmosphere containing an ice cloud layer are 281 and 280 K, respectively, the corresponding τ and

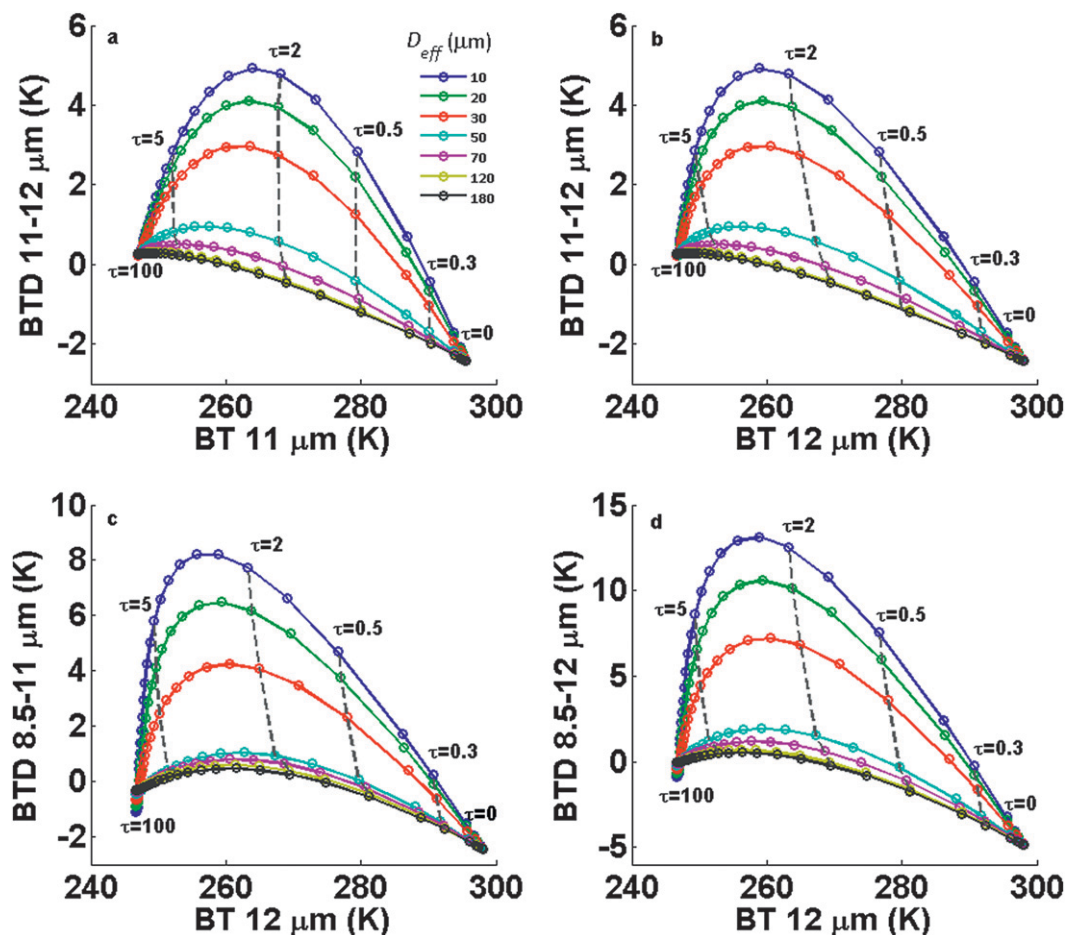


FIG. 4. Simulated TOA BTDs with respect to 11- or 12- μm BTs. The ice cloud is located between 8 and 8.5 km in a generalized tropical atmosphere.

D_{eff} values should be 0.47 and 30 μm according to Fig. 4b. Because of uncertainties from both satellite-measured TOA radiances and the collocation process, however, the TOA BTs are actually 280 and 281 K, respectively. Although the retrieved τ value changes only slightly, the retrieved D_{eff} value is the maximum value of 180 μm , which is 6 times the actual value. In fact, BTD uncertainties are inevitable and arise from incomplete knowledge of the surface emissivity, atmospheric temperature variability, sensor noise, and more (Kahn et al. 2005).

5. Inference of ice cloud properties in satellite data

This section contains the details of the retrieval method, including the datasets used, the retrieval method and results, and the comparisons between the fast-RTM retrieval results and their collection-5 MODIS operational counterparts (“MYD06” products). To implement the retrieval, the cloud-top/cloud-base altitude, background

atmospheric profile, surface emissivity and temperature, TOA radiances at three infrared channels, and μ are necessary. The satellite measurements and retrieval products are selected from 1 January to 31 December 2008, located in the region of 180°W–180°E (around the entire globe) and 80°S–80°N.

The first dataset comes from MODIS, a widely used instrument aboard both the National Aeronautics and Space Administration (NASA) *Terra* and *Aqua* satellites, with 36 spectral bands ranging from 0.41 to 14.5 μm . In the current study, *Aqua*/MODIS level-1B (L1B) collection-5 (“MYD021KM”) data provide TOA radiances for the three IR bands employed as basic input to the IR retrieval procedure. The spatial resolution for MODIS L1B data in IR channels is 1 km at nadir. The *Aqua*/MODIS level-2 cloud products (MYD06) are also used, including the MODIS-retrieved cloud optical thickness (τ_{MODIS}) and effective particle size ($D_{\text{eff,MODIS}}$) values. Note that the cases for which τ_{MODIS} values are

TABLE 1. Datasets used in this study.

Data source	Subset	Quantities selected	Selection criteria
<i>Aqua</i>	MODIS MYD02 (L1B) MODIS MYD06 (L2)	Radiance	Uncertainty $\leq 1\%$
		Cloud fraction	Cloud fraction $> 95\%$
	MODIS cloud phase	Ice phase	
	τ	$\tau < 6.5$	
	D_{eff}	D_{eff} uncertainty $< 30\%$	
<i>CALIPSO</i>	CALIOP 1-km-layer cloud (L2)	Cloud geometry	Cloud-base height ≥ 4.5 km Cloud thickness ≤ 1.5 km Detected cloud layer = 1
		<i>CALIPSO</i> cloud phase	Ice phase
	CALIOP 5-km-layer cloud (L2)	IWP	IWP uncertainty $\leq 30\%$
	IIR track cloud products (L2)	Surface emissivity	
MERRA	Int3_3d_ams_CP	Geopotential height	
		Ozone mixing ratio	
		Surface geopotential	
		Specific humidity	
		Surface pressure	
		Atmosphere temperature	

≥ 6.5 are eliminated because the sensitivity of infrared-based retrieval method is relatively low for such clouds.

In addition to MODIS data, the Cloud-Aerosol Lidar with Orthogonal Polarization (CALIOP) products (“CAL_LID_L2_CLAY”, version 3.01) provide vertical cloud boundaries and thermodynamic phase. The CALIOP is aboard the *Cloud-Aerosol Lidar and Infrared Pathfinder Satellite Observations (CALIPSO)* platform and receives backscatter signals at wavelengths of 532 and 1064 nm. In this study, the *CALIPSO/CALIOP* level-2 cloud-layer products with spatial resolutions of 1 and 5 km are selected to supply comprehensive cloud information, to specify the cloud phase and altitude, and to eliminate the cases having multilayered clouds. To be specific, only geometrically thin ice clouds are selected (i.e., ice cloud geometric thickness is less than 1.5 km). Lidar has the advantage of the ability to detect optically thin clouds; the lidar signal attenuates for opaque clouds ($\tau \geq 3$) (Sassen and Cho 1992; Protat et al. 2006), however. Another instrument on the *CALIPSO* platform is an imaging infrared radiometer (IIR), which provides reference TOA radiances for three infrared channels centered at 8.7, 10.6, and 12 μm . The IIR level-2 track data are selected to provide TOA BTs as reference values for eliminating obvious errors from data collocation because the three infrared channels are similar in wavelength to the selected MODIS channels. Meanwhile, the surface emissivity selected for this study is provided by IIR level-2 track data.

Meteorological profiles are provided by the Modern Era Retrospective-Analysis for Research and Applications

(MERRA) product, which combines both numerical model results and observational data. The 3-h meteorological profiles of temperature, water vapor, and ozone at 42 pressure levels at a horizontal resolution of $1.25^\circ \times 1.25^\circ$ provide information about the background atmosphere.

To compare the retrieval results presented here with the MODIS collection-5 counterparts, referred to as the IR retrievals and MODIS retrievals, respectively, we select the collocated MODIS pixels and *CALIPSO* profiles rigorously (see Table 1 for the details). For instance, we take the third profile from five successive *CALIPSO* profiles that show a single ice cloud layer. A total of 12 900 cases during 2008 remain after filtering to ensure that each of the MODIS pixels is associated with a single ice cloud layer. Figure 5 shows one example of collocated *Aqua/MODIS* and *CALIPSO* images. The MODIS 11- μm granule image is in grayscale, and the green line indicates the *CALIPSO* track. The single-layered ice cloud of interest is enclosed by a red rectangle. The vertical structure provided by the *CALIPSO/CALIOP* 532-nm total backscatter image is also shown in Fig. 6.

The TOA BTs for the three IR bands are simulated on the basis of the fast RTM with MYD06 cloud products as input. The comparisons between simulation results and their MODIS-observed counterparts are shown in Fig. 7. It is interesting to note that the simulation results are systematically underestimated, implying perhaps a difference in assumed ice single-scattering properties, and in the ensuing retrievals,

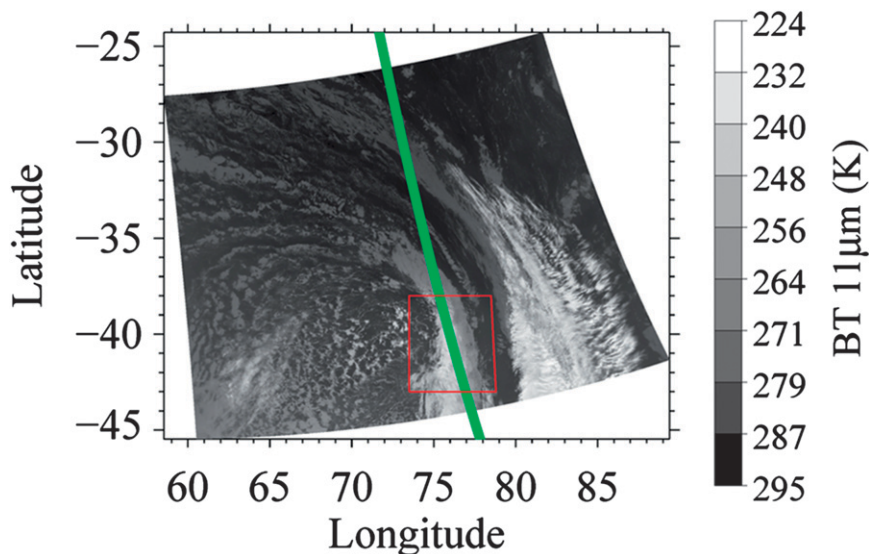


FIG. 5. The 11- μm BT for a MODIS data granule at 0905 UTC 11 Feb 2008. The green line indicates the associated *CALIPSO*/*CALIOP* ground track. The red box indicates the region of interest.

between the solar and IR bands that needs further investigation.

The simulated TOA BTs depend on several parameters, including surface and background atmospheric properties, geometry, and cloud properties. Once other parameters are specified, the cloud properties τ and D_{eff} can be retrieved by making the model simulations fit MODIS observations. To be specific, two retrieval algorithms are implemented for deriving appropriate ice

cloud properties. The first approach employs the Monte Carlo (MC) method to randomly select large numbers of τ - D_{eff} pairs in predetermined ranges (i.e., $-2.0 \leq \log(\tau) \leq 2.0$ and $0 \leq D_{\text{eff}} \leq 180$). The logarithmic scale is used for selecting τ because the IR radiation shows significant sensitivity to τ for optically thin clouds. The τ - D_{eff} pair with the least RMS value is recorded as the most appropriate ice cloud properties. The definition of RMS is shown as follows:

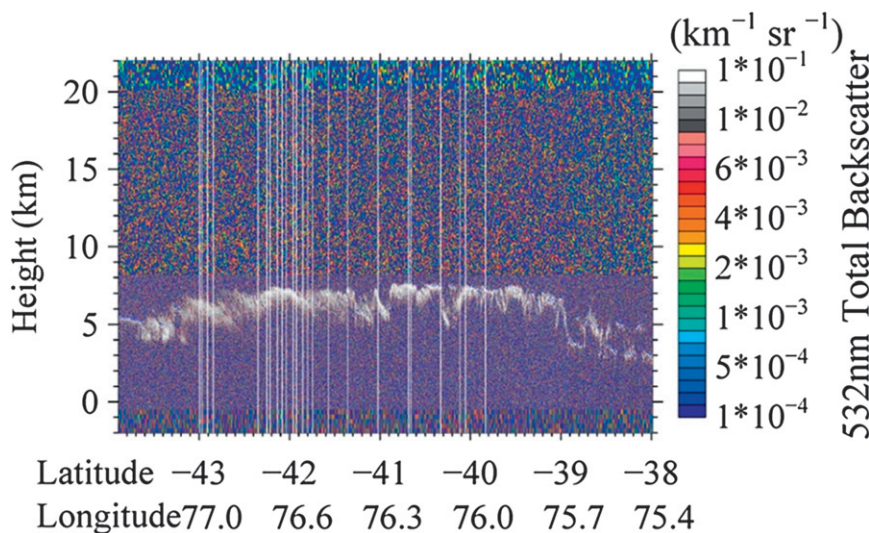


FIG. 6. The *CALIPSO*-detected 532-nm total backscatter along the ground track line within the red box shown in Fig. 5. The white lines indicate the selected profiles.

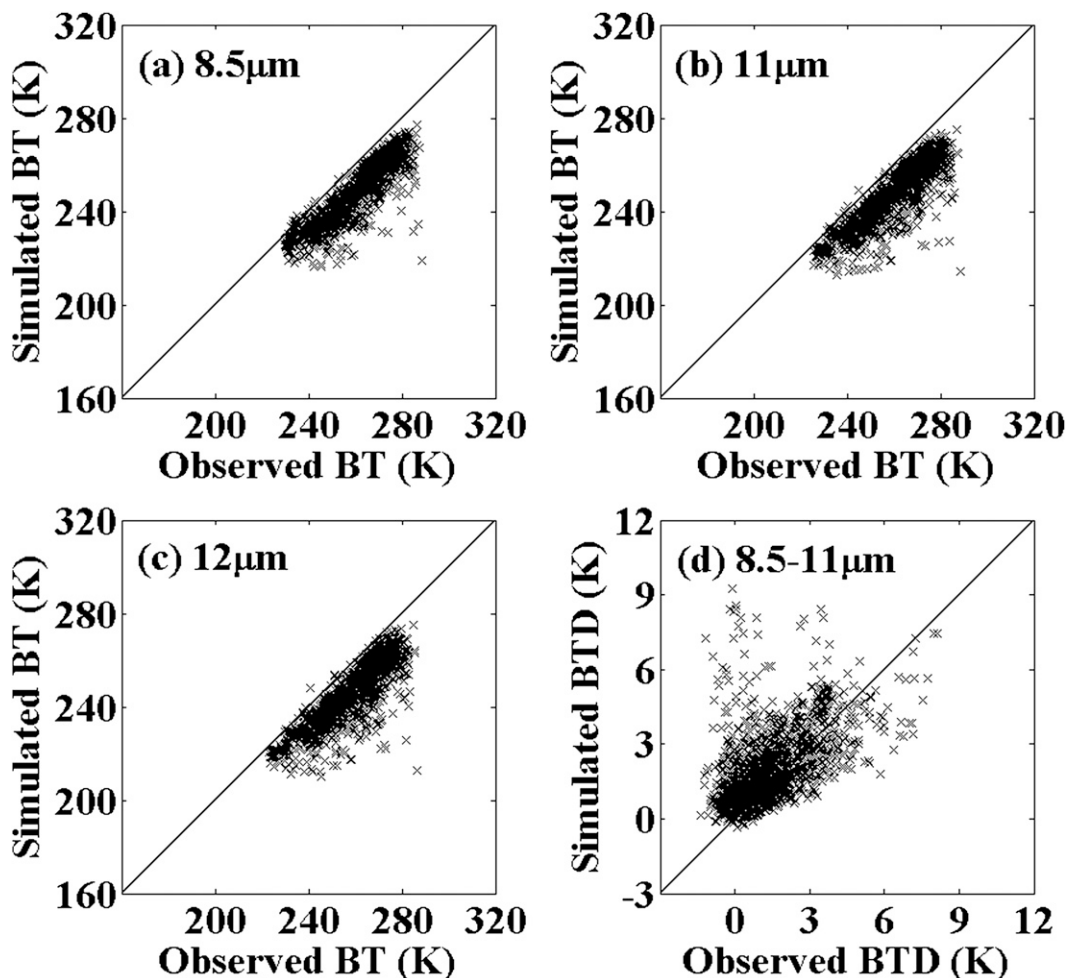


FIG. 7. Scatterplots of MODIS-observed TOA BTs and BTD (8.5–11 μm) vs simulated BTs and BTD by using the MODIS-retrieved τ and D_{eff} .

$$\text{RMS}(\tau, D_{\text{eff}}) = \left[\frac{(\text{BTD}_{o,11-8.5} - \text{BTD}_{s,11-8.5})^2 + (\text{BT}_{o,8.5} - \text{BT}_{s,8.5})^2 + (\text{BT}_{o,12} - \text{BT}_{s,12})^2}{3} \right]^{1/2}, \quad (15)$$

where $\text{BT}_{o,\lambda}$ and $\text{BT}_{s,\lambda}$ are BTs from MODIS observations and the fast-RTM simulations at wavelength λ and $\text{BTD}_{o,11-8.5}$ and $\text{BTD}_{s,11-8.5}$ are the observed and simulated TOA BTDs ($\text{BT}_{11\mu\text{m}} - \text{BT}_{8.5\mu\text{m}}$), respectively.

The second approach chooses τ - D_{eff} pair among preset dense nodes (i.e., 140 and 100 uneven nodes for τ and D_{eff} , respectively). Similar to the MC method, the retrieved τ - D_{eff} pair with least RMS value is chosen as the result. In this study, the second method is employed to conduct the retrieval process because this method provides better results (i.e., smaller RMS can be achieved) than the MC method for the same computing time. This method is

essentially the same as the retrieval technique employed by Garrett et al. (2009), who selected two IR channels to infer τ - D_{eff} pairs for several case studies. Figure 8 shows the simulated TOA BTs and BTD (8.5 – 11 μm) from the retrieved cloud-property pairs versus MODIS observations. In comparison with results from the MODIS operational products shown in Fig. 7, the IR-retrieved cloud-property pairs can provide simulations that closely fit the observations. The mean and standard deviation of RMS for 1290 cases are 0.43 and 0.35 K, respectively.

The scatterplots comparing the MODIS operational cloud properties and the IR retrievals are shown in

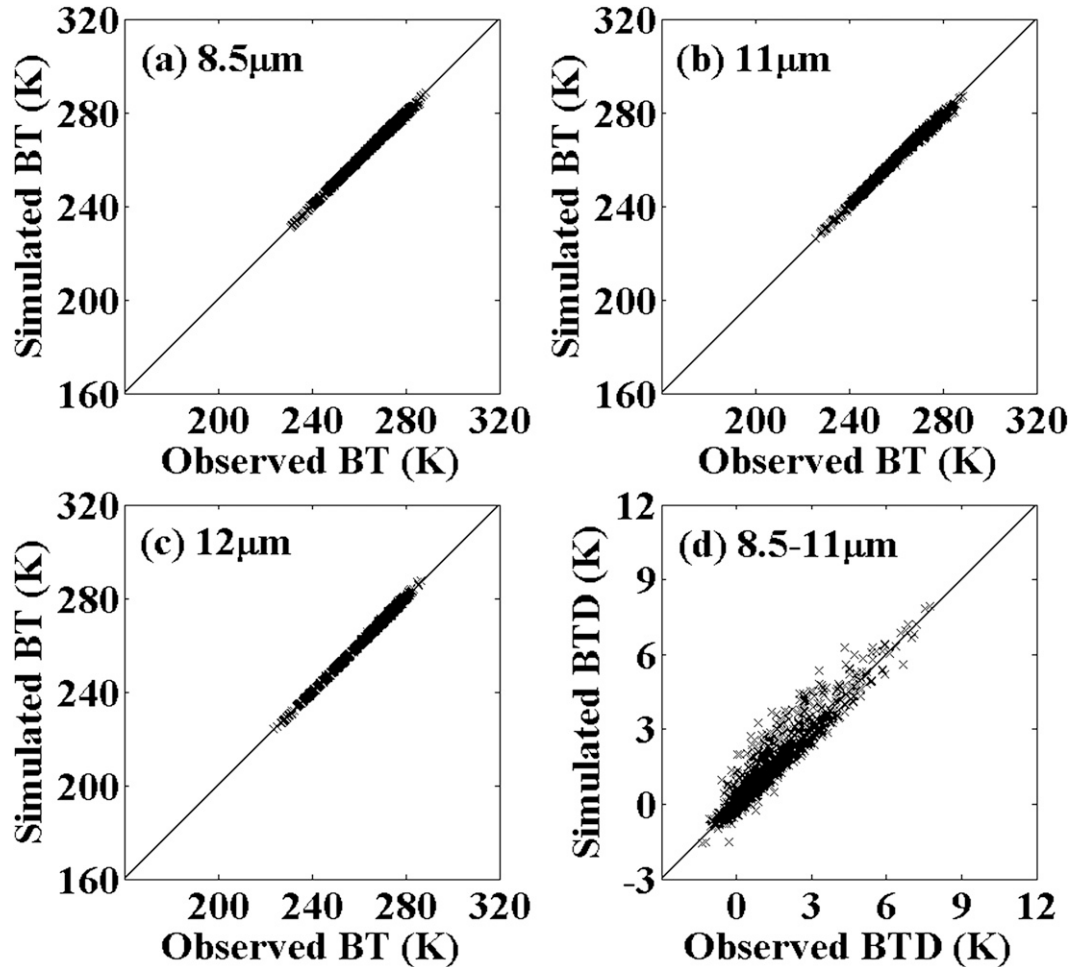


FIG. 8. As in Fig. 7, but the simulated TOA BTs/BTD are calculated using IR-retrieved cloud properties.

Fig. 9. The IR-retrieved cloud optical thickness values τ_{IR} are systematically smaller than their MODIS counterparts τ_{MODIS} . Moreover, τ_{MODIS} spans a large range from 1 to 6.5, whereas τ_{IR} has a relatively narrower distribution. Approximately 90% of the τ_{IR} values are smaller than 4. The comparison between retrieved effective particle size values $D_{eff,IR}$ and their MODIS counterparts $D_{eff,MODIS}$ is shown in Fig. 9b. The $D_{eff,IR}$ mean of $55.3 \mu\text{m}$ is slightly less than the mean of $D_{eff,MODIS}$ ($58.5 \mu\text{m}$). The retrieval performance details are shown in Table 2. Figures 10 and 11 show the distributions of both MODIS and fast-model-retrieved cloud properties. According to the sensitivity study, if $D_{eff,IR} > 120 \mu\text{m}$, the retrieved values are likely inaccurate since there is little sensitivity to very large particle size values. Therefore, in this study, these cloud effective particle sizes are eliminated (less than 5% of the 1290 cases).

Moreover, *CALIPSO* ice water content/path (IWC/IWP) is selected as a reference parameter to explore the accuracy of IR retrievals. IWC/IWP provided by

CALIPSO is considered as a function of the temperature and volume extinction coefficient (Heymsfield et al. 2005) in the form of

$$IWC = a\sigma^b, \tag{16}$$

where a and b are two coefficients that depend upon temperature. The relationship among τ , D_{eff} , and IWC/IWP is shown as follows:

$$IWC(z) = \rho_i \int_{D_{min}}^{D_{max}} V(D, z)n(D, z) dD, \tag{17}$$

where z is a given altitude and ρ_i is the density of solid ice (approximately $9.168 \times 10^5 \text{ g m}^{-3}$). The cloud optical thickness can be expressed as

$$\tau = \int_{\text{cloudbase}}^{\text{cloudtop}} \int_{D_{min}}^{D_{max}} Q_e A(D, z)n(D, z) dD dz, \tag{18}$$

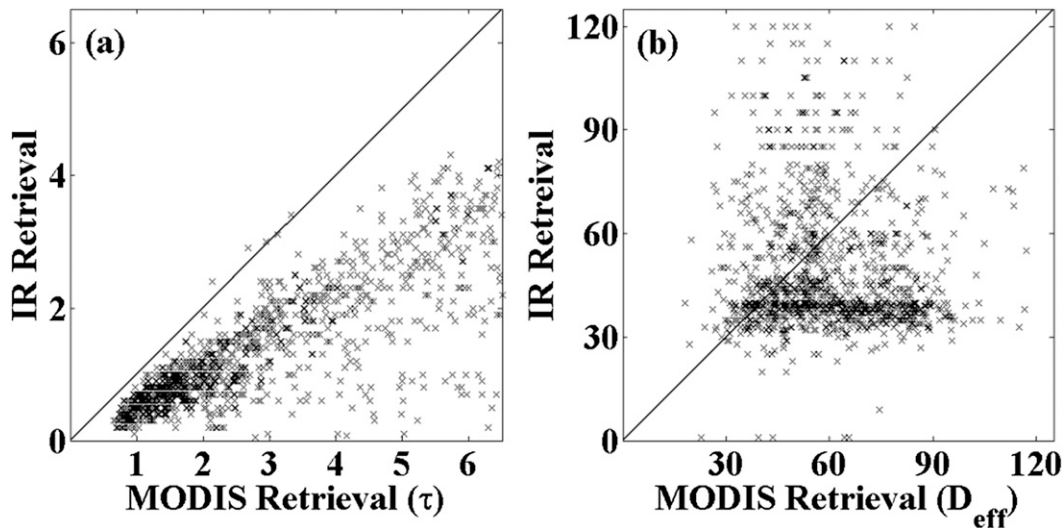


FIG. 9. Scatterplots of MODIS-observed cloud optical properties vs the IR-retrieved results.

and, with the definition of D_{eff} given by Eq. (2), IWP can be represented as follows:

$$\text{IWP} = \int_{\text{cloudbase}}^{\text{cloudtop}} \text{IWC}(z) dz = \frac{2\tau\rho_i D_{\text{eff}}}{3\langle Q_e \rangle}, \quad (19)$$

where $\langle Q_e \rangle$ is the bulk average extinction efficiency. Because τ is the cloud optical thickness for a visible channel, the particle size is assumed to be much larger than the wavelength. Therefore, $\langle Q_e \rangle$ is assumed to be 2 in this study. Equation (19) can be rewritten as

$$\text{IWP} = (D_{\text{eff}}\rho_i\tau)/3, \quad (20)$$

where the units of D_{eff} and IWP are micrometers and grams per meter squared, respectively. Therefore, the comparison between the IR-retrieved IWP_{IR} [Eq. (20)] and *CALIPSO*-retrieved IWP_{CAL} [Eq. (16)] is shown in Fig. 12. It is found that these two kinds of products show robust agreement for much of the IWP range. For larger IWP values, the IWP_{IR} are slightly greater than their *CALIPSO* counterparts, which may result from the significant attenuation of the lidar signal in the relatively opaque ice clouds. The uncertainties of the selected *CALIPSO* IWP products are limited to 30%. For the IR-retrieved IWP, the error is essentially proportional to the errors from τ and D_{eff} . In general, regardless of the error sources from the fast model and satellite observations, the major sources of error come from the low sensitivity of applying an IR method to infer properties for an optically thick cloud with large D_{eff} and from the

vertically inhomogeneous feature of the size distribution of ice crystals (Zhang et al. 2010). All of these issues need further study.

6. Discussion and conclusions

Our study develops a fast IR RTM to simulate the TOA BTs of three MODIS IR bands (8.5, 11, and 12 μm) for ice cloud conditions. The differences found from comparisons between this model and the more rigorous DISORT are generally less than 0.1 K, but the fast RTM runs 6000 times as fast as the DISORT + CKD method on a desktop computer. The main difference between this model and other reported fast RT models, such as FIRT M1 and FIRT M2, is the inclusion of two LUTs that provide cloud effective emissivity and effective temperature functions.

The LUT of cloud effective temperature improves the accuracy of the model significantly, in particular for simulating TOA BTs in an atmosphere containing a transmissive cloud layer. For instance, for an optically thin cloud ($\tau < 3$), the internal part of the cloud also significantly contributes to the emitted radiance at cloud top. For this reason, it is important to find a relationship

TABLE 2. Comparison of MODIS retrievals with the IR retrievals.

Method	Mean of τ	Mean of D_{eff} (μm)	Mean of RMS_{BTD} (K)	Std dev of RMS_{BTD} (K)
MODIS retrieval	2.83	58.5	10.82	5.8
IR retrieval	1.39	55.3	0.43	0.35

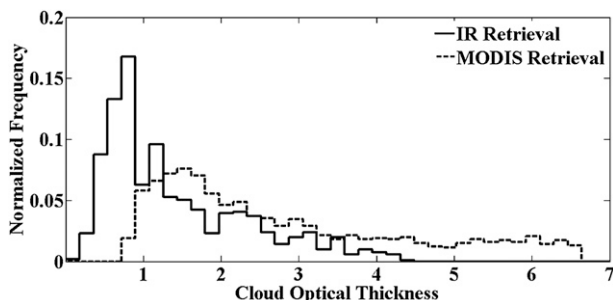


FIG. 10. Ice cloud optical thickness distribution given by the IR retrieval and MODIS.

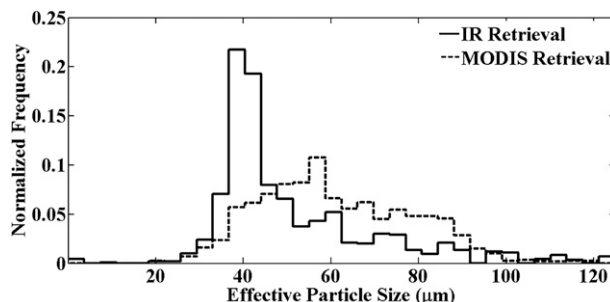


FIG. 11. Ice cloud effective particle size distribution given by the IR retrieval and MODIS.

between the cloud-top/cloud-base temperature and cloud emission. On the basis of the LUT of cloud effective temperature, the fast model computes cloud-top upwelling radiance (or cloud-base downwelling radiance) efficiently and accurately. Some deficiencies in this RTM limit the application and accuracy of the model, however. For example, this model cannot be applied to the multilayered cloud or liquid water/mixing-phase cloud situations. Furthermore, considerable errors occur when scattering processes are important (i.e., at $8.5 \mu\text{m}$ when small ice particles dominate), suggesting that the fast RTM does not capture scattering processes accurately.

With the cloud geometry inferred from *CALIPSO*, this computationally efficient RTM may be applied to retrievals of τ and D_{eff} from both multispectral satellite imagery and hyperspectral IR sounder data. The inference of ice cloud properties on the basis of the fast RTM is applicable to both daytime and nighttime data because only IR channels are involved. Furthermore, the sensitivity study suggests that the radiances of the IR-window wavelengths are sensitive to small τ and D_{eff} ; whereas the solar-reflectance method has more sensitivity to optically thick ice clouds containing larger particles. The comparisons between IR retrieval results and the MODIS operational collection-5 cloud products indicate that, for the τ retrieval, the MODIS products tend to give larger values than the IR retrieval for most cases ($\tau_{\text{MODIS}} < 6.5$) whereas the IR-retrieved D_{eff} values are smaller than their MODIS counterparts. Because the absorption processes are dominant for ice clouds in the IR region, the IR retrieval results are less sensitive to particle shape distribution and vertical structure, which implies that the IR retrieval gives more reliable ice cloud properties than do the MODIS collection-5 products for optically thin ice clouds with relatively small particles.

Several researchers report anomalously high numbers of small ice crystals in in situ measurements as a result of shattering and collision processes and the consequential impacts on parameterization of ice

crystals (e.g., Mitchell and d'Entremont 2008; Mitchell et al. 2010). Some studies indicate that the scattering features at VIS/SWIR channels are sensitive to ice cloud PSD, habits distribution, and the degree of roughness (e.g., Hess et al. 1998; Sun et al. 2004; Yang et al. 2008; Baum et al. 2010), whereas in the IR region strong absorption reduces these effects (Yang et al. 2005). Another factor that has an impact on both VIS/SWIR and IR retrieval methods arise from the vertical inhomogeneity of effective particle size distribution within the ice cloud layer (Zhang et al. 2010). In general, these impacts need further study. The IR retrieval method is complementary to the VIS/SWIR method because of its sensitivity to optically thin ice cloud optical thickness and effective particle size and its lack of dependence on solar illumination.

Acknowledgments. This study was partially supported by NASA Grant NNX08AP57G. Bryan Baum and Ping Yang gratefully acknowledge the support provided through NASA Grant NNX11AF40G. The views, opinions, and findings contained in this report are those of the authors and should not be construed as an official National Oceanic and Atmospheric Administration or U.S. government position, policy, or decision.

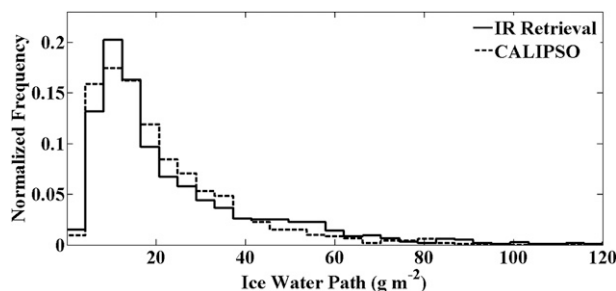


FIG. 12. Ice water path distribution given by the IR retrieval and *CALIPSO*.

REFERENCES

- Baran, A. J., 2004: On the scattering and absorption properties of cirrus cloud. *J. Quant. Spectrosc. Radiat. Transfer*, **89**, 17–36.
- , 2009: A review of the light scattering properties of cirrus. *J. Quant. Spectrosc. Radiat. Transfer*, **110**, 1239–1260.
- Baum, B. A., R. A. Frey, G. G. Mace, M. K. Harkey, and P. Yang, 2003: Nighttime multilayered cloud detection using MODIS and ARM data. *J. Appl. Meteor.*, **42**, 905–919.
- , A. J. Heymsfield, P. Yang, and S. T. Bedka, 2005a: Bulk scattering properties for the remote sensing of ice clouds. Part I: Microphysical data and models. *J. Appl. Meteor.*, **44**, 1885–1895.
- , P. Yang, A. J. Heymsfield, S. Platnick, M. D. King, Y. X. Hu, and S. T. Bedka, 2005b: Bulk scattering properties for the remote sensing of ice clouds. Part II: Narrowband models. *J. Appl. Meteor.*, **44**, 1896–1911.
- , —, S. L. Nasiri, A. K. Heidinger, A. J. Heymsfield, and J. Li, 2007: Bulk scattering properties for the remote sensing of ice clouds. Part III: High-resolution spectral models from 100 to 3250 cm^{-1} . *J. Appl. Meteor. Climatol.*, **46**, 423–434.
- , —, Y. X. Hu, and Q. Feng, 2010: The impact of ice particle roughness on the scattering phase matrix. *J. Quant. Spectrosc. Radiat. Transfer*, **111**, 2534–2549.
- Chepfer, H., G. Brogniez, and Y. Fouquart, 1998: Cirrus clouds' microphysical properties deduced from POLDER observations. *J. Quant. Spectrosc. Radiat. Transfer*, **60**, 375–390.
- Chiriaco, M., H. Chepfer, V. Noel, A. Delaval, M. Haefelin, P. Dubuisson, and P. Yang, 2004: Improving retrievals of cirrus cloud particle size coupling lidar and three-channel radiometric techniques. *Mon. Wea. Rev.*, **132**, 1684–1700.
- Collins, D. G., W. G. Blättner, M. B. Wells, and H. G. Horak, 1972: Backward Monte Carlo calculations of the polarization characteristics of the radiation emerging from spherical-shell atmospheres. *Appl. Opt.*, **11**, 2684–2696.
- Dubuisson, P., V. Giraud, O. Chomette, H. Chepfer, and J. Pelon, 2005: Fast radiative transfer modeling for infrared imaging radiometry. *J. Quant. Spectrosc. Radiat. Transfer*, **95**, 201–220.
- Garrett, K. J., P. Yang, S. L. Nasiri, C. R. Yost, and B. A. Baum, 2009: Influence of cloud-top height and geometric thickness on a MODIS infrared-based ice cloud retrieval. *J. Appl. Meteor. Climatol.*, **48**, 818–832.
- Hansen, J. E., and J. W. Hovenier, 1971: The doubling method applied to multiple scattering of polarized light. *J. Quant. Spectrosc. Radiat. Transfer*, **11**, 809–812.
- Heidinger, A. K., and M. J. Pavolonis, 2009: Gazing at cirrus clouds for 25 years through a split window. Part I: Methodology. *J. Appl. Meteor. Climatol.*, **48**, 1100–1116.
- , C. O'Dell, R. Bennartz, and T. Greenwaldand, 2006: The successive-order-of-interaction radiative transfer model. Part I: Model development. *J. Appl. Meteor. Climatol.*, **45**, 1388–1402.
- Hess, M., R. B. A. Koelemeijer, and P. Stammes, 1998: Scattering matrices of imperfect hexagonal ice crystals. *J. Quant. Spectrosc. Radiat. Transfer*, **60**, 301–308.
- Heymsfield, A. J., A. Bansemmer, P. R. Field, S. L. Durden, J. L. Stith, J. E. Dye, W. Hall, and C. A. Grainger, 2002: Observations and parameterizations of particle size distributions in deep tropical cirrus and stratiform precipitating clouds: Results from in situ observations in TRMM field campaigns. *J. Atmos. Sci.*, **59**, 3457–3491.
- , D. M. Winker, and G.-J. Zadelhoff, 2005: Extinction-ice water content-effective radius algorithms for CALIPSO. *Geophys. Res. Lett.*, **32**, L10807, doi:10.1029/2005GL022742.
- Hong, G., P. Yang, H. L. Huang, B. A. Baum, Y. X. Hu, and S. Platnick, 2007: The sensitivity of ice cloud optical and microphysical passive satellite retrievals to cloud geometrical thickness. *IEEE Trans. Geosci. Remote Sens.*, **45**, 1315–1323.
- Inoue, T., 1985: On the temperature and effective emissivity determination of semitransparent cirrus clouds by bi-spectral measurements in the 10 μm window region. *J. Meteor. Soc. Japan*, **63**, 88–89.
- Kahn, B. H., and Coauthors, 2005: Nighttime cirrus detection using Atmospheric Infrared Sounder window channels and total column water vapor. *J. Geophys. Res.*, **110**, D07203, doi:10.1029/2004JD005430.
- Kokhanovsky, A. A., and T. Nauss, 2005: Satellite-based retrieval of ice cloud properties using a semianalytical algorithm. *J. Geophys. Res.*, **110**, D19206, doi:10.1029/2004JD005744.
- Kratz, D. P., 1995: The correlated k -distribution technique as applied to the AVHRR channels. *J. Quant. Spectrosc. Radiat. Transfer*, **53**, 501–517.
- , and F. G. Rose, 1999: Accounting for molecular absorption within the spectral range of the CERES window channel. *J. Quant. Spectrosc. Radiat. Transfer*, **61**, 83–95.
- Liu, X., W. L. Smith, D. K. Zhou, and A. Larar, 2006: Principal component-based radiative transfer model for hyperspectral sensors. *Appl. Opt.*, **45**, 201–209.
- McMillin, L. M., T. J. Kleespies, and L. J. Crone, 1995: Atmospheric transmittance of an absorbing gas. 5. Improvements to the OPTRAN approach. *Appl. Opt.*, **34**, 8396–8399.
- Minnis, P., and Coauthors, 2011a: CERES edition-2 cloud property retrievals using TRMM VIRS and Terra and Aqua MODIS data—Part I: Algorithms. *IEEE Trans. Geosci. Remote Sens.*, doi:10.1109/TGRS.2011.2144601, in press.
- , and Coauthors, 2011b: CERES edition-2 cloud property retrievals using TRMM VIRS and Terra and Aqua MODIS data—Part II: Examples of average results and comparisons with other data. *IEEE Trans. Geosci. Remote Sens.*, doi:10.1109/TGRS.2011.2144602, in press.
- Mitchell, D. L., 2002: Effective diameter in radiative transfer: General definition, application, and limitations. *J. Atmos. Sci.*, **59**, 2330–2346.
- , and R. P. d'Entremont, 2008: Satellite remote sensing of small ice crystal concentrations in cirrus clouds. *Proc. 15th Int. Conf. on Clouds and Precipitation*, Cancun, Mexico, ICCP, 185–188.
- , —, and R. P. Lawson, 2010: Inferring cirrus size distributions through satellite remote sensing and microphysical databases. *J. Atmos. Sci.*, **67**, 1106–1125.
- Moncet, J. L., G. Uymin, A. E. Lipton, and H. E. Snell, 2008: Infrared radiance modeling by optimal spectral sampling. *J. Atmos. Sci.*, **65**, 3917–3934.
- Nakajima, T., and M. D. King, 1990: Determination of the optical thickness and effective particle radius of clouds from reflected solar radiation measurements. Part I: Theory. *J. Atmos. Sci.*, **47**, 1878–1893.
- Niu, J., P. Yang, H. L. Huang, J. E. Davies, J. Li, B. A. Baum, and Y. X. Hu, 2007: A fast infrared radiative transfer model for overlapping clouds. *J. Quant. Spectrosc. Radiat. Transfer*, **103**, 447–459.
- Plass, G. N., and G. W. Kattawar, 1968: Monte Carlo calculation of light scattering from clouds. *Appl. Opt.*, **7**, 415–419.
- Platnick, S., M. D. King, S. A. Ackerman, W. P. Menzel, B. A. Baum, J. C. Riédi, and R. A. Frey, 2003: The MODIS cloud products: Algorithms and examples from Terra. *IEEE Trans. Geosci. Remote Sens.*, **41**, 459–473.
- Prabhakara, C., R. S. Fraser, G. Dalu, M.-L. C. Wu, R. J. Curran, and T. Styles, 1988: Thin cirrus clouds: Seasonal distribution

- over oceans deduced from *Nimbus-4* IRIS. *J. Appl. Meteor.*, **27**, 379–399.
- Protat, A., A. Armstrong, M. Haeffelin, Y. Morille, J. Pelon, J. Delanoë, and D. Bouniol, 2006: Impact of conditional sampling and instrumental limitations on the statistics of cloud properties derived from cloud radar and lidar at SARTA. *Geophys. Res. Lett.*, **33**, L11805, doi:10.1029/2005GL025340.
- Sassen, K., and B. S. Cho, 1992: Subvisual-thin cirrus lidar dataset for satellite verification and climatological research. *J. Appl. Meteor.*, **31**, 1275–1285.
- Saunders, R., M. Matricardi, and P. Brunel, 1999: An improved fast radiative transfer model for assimilation of satellite radiance observations. *Quart. J. Roy. Meteor. Soc.*, **125**, 1407–1425.
- , P. Brunel, S. English, P. Bauer, U. O’Keeffe, P. Francis, and P. Rayer, 2006: RTTOV-8—Science and validation report. Met Office Forecasting and Research Tech. Doc. NWPSAF-MO-TV-007, 46 pp.
- Stamnes, K., S. C. Tsay, W. Wiscombe, and K. Jayaweera, 1988: Numerically stable algorithm for discrete-ordinate-method. *Appl. Opt.*, **27**, 2502–2509.
- Stubenrauch, C. J., R. E. Holz, A. Chedin, D. L. Mitchell, and A. J. Baran, 1999: Retrieval of cirrus ice crystal sizes from 8.3 and 11.1 μm emissivities determined by the improved initialization inversion of TIROS-N operational vertical sounder observations. *J. Geophys. Res.*, **104**, 793–808.
- Sun, W., N. G. Loeb, G. Videen, and Q. Fu, 2004: Examination of surface roughness on light scattering by long ice columns by use of a two-dimensional finite-difference time-domain algorithm. *Appl. Opt.*, **43**, 1957–1964.
- Twomey, S., N. Jacobowitz, and H. B. Howell, 1966: Matrix methods for multiple-scattering problems. *J. Atmos. Sci.*, **23**, 289–296.
- Warren, S. G., and R. E. Brandt, 2008: Optical constants of ice from the ultraviolet to the microwave: A revised compilation. *J. Geophys. Res.*, **113**, D14220, doi:10.1029/2007JD009744.
- Wei, H., P. Yang, J. Li, B. A. Baum, H. L. Huang, S. Platnick, Y. X. Hu, and L. Strow, 2004: Retrieval of semitransparent ice cloud optical thickness from Atmospheric Infrared Sounder (AIRS) measurements. *IEEE Trans. Geosci. Remote Sens.*, **42**, 2254–2266.
- Wendisch, M., and Coauthors, 2005: Impact of cirrus crystal shape on solar spectral irradiance: A case study for subtropical cirrus. *J. Geophys. Res.*, **110**, D03202, doi:10.1029/2004JD005294.
- Yang, P., K. N. Liou, K. Wyser, and D. L. Mitchell, 2000: Parameterization of the scattering and absorption properties of individual ice crystals. *J. Geophys. Res.*, **105**, 4699–4718.
- , H. Wei, H. L. Huang, B. A. Baum, Y. X. Hu, G. W. Kattawar, M. I. Mishchenko, and Q. Fu, 2005: Scattering and absorption property database for nonspherical ice particles in the near-through far-infrared spectral region. *Appl. Opt.*, **44**, 5512–5523.
- , L. Zhang, G. Hong, S. L. Nasiri, B. A. Baum, H. L. Huang, M. D. King, and S. Platnick, 2007: Differences between collection 004 and 005 MODIS ice cloud optical/microphysical products and their impact on radiative forcing simulations. *IEEE Trans. Geosci. Remote Sens.*, **45**, 2886–2899.
- , G. W. Kattawar, G. Hong, P. Minnis, and Y. X. Hu, 2008: Uncertainties associated with the surface texture of ice particles in satellite-based retrieval of cirrus clouds: Part I. Single-scattering properties of ice crystals with surface roughness. *IEEE Trans. Geosci. Remote Sens.*, **46**, 1940–1947.
- Zhang, Z., P. Yang, G. W. Kattawar, S.-C. Tsay, B. A. Baum, Y. Hu, A. J. Heymsfield, and J. Reichardt, 2004: Geometrical-optics solution to light scattering by droxtal ice crystals. *Appl. Opt.*, **43**, 2490–2499.
- , and Coauthors, 2007: A fast infrared radiative transfer model based on the adding–doubling method for hyperspectral remote-sensing applications. *J. Quant. Spectrosc. Radiat. Transfer*, **105**, 243–263.
- , S. Platnick, P. Yang, A. K. Heidinger, and J. M. Comstock, 2010: Effects of ice particle size vertical inhomogeneity on the passive remote sensing of ice clouds. *J. Geophys. Res.*, **115**, D17203, doi:10.1029/2010JD013835.